PHYTOPLANKTON DISTRIBUTION IN THE MIXED LAYER: IMPLICATION TO KRILL ABUNDANCE*

Hidekatsu Yamazaki and Thomas R. Osborn

Abstract

A one dimensional Lagrangian model of random walk is presented to study the distribution of phytoplankton in the Antarctic ocean. Since little is known about mixed layer dynamics in the Antarctic Ocean, we estimate the depth of the mixed layer and its turbulence intensity from an Ekman layer model. Available CTD data suggest that the mixing in the upper layer is less than what we expected. However, the effect on the dynamics is vital, affecting the distribution of particles in the upper ocean.

Résumé

Un modèle uni-dimensionnel de trajet aléatoire de Lagrange est présenté pour permettre l'étude de la distribution du phytoplancton dans l'océan Antarctique. Vu que l'on possède une connaissance réduite de la dynamique des couches mixtes dans l'océan Antarctique, la profondeur de la couche mixte et l'intensité de sa turbulence ont été estimées d'après un modèle de couche d'Ekman. Des données disponibles de conductivité, température, profondeur, suggèrent que le mélange dans la couche supérieure est moindre que l'on ne s'y attendait. Cependant, la répercussion sur la dynamique est vitale, car elle modifie la distribution des particules dans la couche supérieure de l'océan.

Резюме

Для изучения распространения фитопланктона в водах Антарктики представлена одномерная модель Лагренджа (Lagrange) случайного блуждания. Поскольку мало известно о динамике смешанного слоя в водах Антарктики, глубина смешанного слоя и интенсивность турбулентности в нем были оценены с помощью модели слоя Экмана (Ekman layer model). По имеющимся данным по проводимости, температуре и глубине (CTD) можно предположить, что смешение в верхнем слое меньше предполагаемого. Тем не менее, его воздействие на динамику велико, в связи с тем, что оно оказывает влияние на распределение частиц в верхних слоях океана.

Resumen

Se presenta un modelo unidimensional de Lagrange de trayecto aleatorio para estudiar la distribución del fitoplancton en el Océano

* (Revised)

Antártico. Ya que se sabe poco sobre la dinámica de las capas mixtas del Océano Antártico, estimamos la profundidad de la capa mixta y su intensidad de turbulencia a partir de un modelo de la capa Ekman. Los datos CTD disponibles, sugieren que la mezcla en la capa superior es menor de lo esperado. Sin embargo, el efecto en la dinámica es vital, afectando a la distribución de partículas en la parte superior del océano.

1. INTRODUCTION

There has been an increasing interest in the variability of biological marine resources, but little progress toward accurate predictions of productivity has been made. The major difficulty arises in variations among the density-dependent populations whose controlling factors are not only the prey-predator interaction and the physiological conditions but also the *in situ* physical environment. The problem, as it now stands, is highly complex with many degrees of freedom.

The basic concept underlying our approach is to use a Lagrangian kinematic model to trace individual organisms in space and time. Historically, Eulerian models have been adapted to study the distribution of plankton. For example, Wroblewski (1982) models copepoda abundance during upwelling off the Oregon coast. The model results agree favorably with observations. Since the Eulerian models inherently deal with averaged spatial distributions, the results may differ considerably from the reality because physical-biological interactions are highly non-linear. Woods and Onken (1982) state that "averaging non-linear equations before integration does not give the same answer as averaging them after integration." An individual life history can only be evaluated by a Lagrangian type model. They also note that "..the power of the Lagrangian ensemble method lies in its potential for testing the consequences of different hypotheses concerning the physiology and behavior of plankton, in a systematic and internally consistent way". They are referring to phytoplankton but the same principal holds for zooplankton. Platt and Gallegos (1980) state that "we need more knowledge about how complex trajectories affect photosynthetic performance by phytoplankton; we need to incorporate these complex trajectories into our experimental designs; and we need to cooperate with physical oceanographer to study how the temporal responses to the phytoplankton are coupled to the temporal scales of mixing found in nature". Lagrangian models require an extensive computational effort compared to Eulerian models, but the models have advantages; namely the coding does not require a sophisticated algorithm; the model can be fairly flexible to variety of environmental conditions; and prey-predator interaction can be "directly" evaluated by the model. Recent advancements of computer technology make the operation time less significant.

Although experiments suggest that krill are omnivorous, the animals extensively feed on phytoplankton. Boyd et al. (1984) estimate that they spend up to 30% of their total respiratory energy collecting food. Morris et al. (1984) suggest that the turnover rate of chlorophyll in a krill's stomach is of the order of minutes. These reports imply that krill are continuously grazing, and that females must continuously consume food to meet the minimum requirement for the production of eggs. To meet the minimum nutrient level they must find high concentrations of food. Another important process is the efficiency of the food capturing and handling. Ross and Quetin (1986) suggest that schooling and swimming behavior of krill may be related to foraging. A strategy to minimize energy requirement for feeding would be expected. A correlation between krill swarms and phytoplankton abundance was discussed by Weber and El-Sayed (1985). Hence, we think that studying the distribution of the food (phytoplankton) is the key to understanding the distribution of krill. The animals are excellent swimmers and velocities of 40 cm s^{-1} are possible. Therefore, small scale turbulence is irrelevant to their swimming ability, but the turbulence can significantly affect the distribution of their food source and their foraging. The goal of our study is to develop a Lagrangian prey-predator model for krill and phytoplankton. Phytoplankton grow in the upper ocean where enhanced mixing due to turbulence can be found. Unfortunately, however, very little is known about mixed layers in the Antarctic ocean.

We deduce the dynamics of the mixed layer in the Antarctic ocean from existing STD data in the next section. Implementation of one-dimensional Lagrangian model is discussed in section 3. The last section summarizes our preliminary results.

2. THE MIXED LAYER IN THE ANTARCTIC

2.1 STD Data

STD data from a hydrographic survey made from R/V *Professor Seidlecki* in January, 1987 near the Antarctic Peninsula were used to investigate the level of turbulence in the mixed layer. A section along 57° W (Figure 1) shows the transition from Pacific water to Bransfield Strait water separated by a frontal zone at near the latitude 61.3 degrees south (Gordon, 1988). In general, the stratification in the Antarctic Ocean, south of the front, is very weak compared to that of the low latitude ocean. The depths of the mixed layer in the Pacific water, north of the front, ranges between 30 and 50 meters. A sharp pycnocline near 40 m in STD237 shows a high buoyancy frequency, N, as is often found at the base of mixed layers at mid-latitude. Stratification in the continental front and Bransfield strait water is weak, and mixed layers are not apparent. Since wind speeds were typically 10 to 15 m s^{-1} (Chapman, personal communication), the buoyancy flux provided by melt water must be suppressing the surface mixing. The Weddell Sea is covered by the sea ice in January.

2.2 Mixed Layer Depth

The depth of mixing is controlled by the surface buoyancy production (cooling promotes convection) and by the surface wind stress, but quantitative relationships between the depth of mixing and surface forcing are still controversial. Since very little is known about surface forcing in the Antarctic ocean, we will use the Ekman depth

$$h_E = \kappa u_*/f \qquad (1)$$

as the upper limit to the depth of mixing, where $u_* = (t_o/\rho)^{1/2}$, t_o is the surface wind stress, f the Coriolis parameter and ρ the density of water. Turbulence observations at mid-latitudes for wind speeds of 10 m s^{-1} show mixing to approximately 65% of the Ekman depth (Lueck, 1989). Because of the strong surface buoyancy flux provided by melt water, convective mixing is not expected during the southern summer. For current models, the Ekman depth is a sufficient indicator of the depth of mixing.

2.3 Turbulence

Under purely wind-stress forcing, the rate of dissipation of kinetic energy should follow

$$\varepsilon = u_*^3/\kappa z \qquad (2)$$

(Gregg, 1987). Figure 2 shows the dissipation profile for U_{10} = 1, 5, 10 and 20 m sec^{-1} at 61°S and the profiles are terminated at the depth of Ekman layer. The dissipation rate decreases inversely from 5×10^{-6} W kg^{-1} at 1 meter to 10^{-7} W kg^{-1} for U_{10}=10 m sec^{-1}. The average dissipation rate $\langle\varepsilon\rangle$ over the depth range gives 5×10^{-7} W kg^{-1}. In order to exam the scale of turbulent mixing we introduce a universal spectrum for the isotropic turbulence. The energy spectrum $E(k)$ is expressed as follows

$$E(k) = \alpha\varepsilon^{2/3}k^{-5/3}\exp[-1.5\alpha\{\pi\beta\alpha^{-1/2}(kl)^{-4/3}+(k\eta)^{4/3}\}] \qquad (3)$$

where α and β are canonical constants and k is the radian wave number. The spectrum shape has a sharp cut-off at both the energy containing eddy scale l and the Kolmogorov length scale $\eta\equiv(\nu^3/\varepsilon)^{1/4}$. For a scale smaller than $2\pi\eta$ the flow is dominated by the viscosity and is laminar. The integration of $E(k)$ gives the turbulence kinetic energy $q^2\equiv3u^2/2$,

$$q^2 = \int_0^\infty E(k)\, dk \qquad (4)$$

where u is the rms turbulent velocity scale.

The dissipation rate spectrum $D(k)$ can be expressed in terms of $E(k)$ as follows

$$D(k) = 2\nu k^2 E(k) \qquad (5)$$

The integration of $D(k)$ gives the kinetic dissipation rate.

$$\varepsilon = \int_0^\infty D(k)\, dk \qquad (6)$$

The dissipation rate can be set from the Ekman layer model. The dissipation rate is also related to the energy containing eddy scale.

$$\varepsilon = A u^3 l^{-1} \qquad (7)$$

where A is a constant of an order one. For the sake of simplicity we have used $A=1$. Therefore by knowing ε, for our case $<\varepsilon>$ from the Ekman layer model, u can be evaluated with l.

The energy containing eddy scale, l, is bounded by the depth of mixed layer and may be proportional the Ozmidov scale $L_o \equiv (\varepsilon N^{-3})^{1/2}$ which is a scale of the largest eddy size in a stratified fluid. Stratification limits the vertical scale of turbulent fluctuations although not necessarily the vertical extent of the patches. Detailed measurements of the three turbulent velocity components (Gargett et al. 1984) from the *Pisces* submersible show the suppression of vertical velocities at scale larger than L_o. The turbulence velocity scale u may be estimated by assuming $l \approx L_o$.

$$u = (<\varepsilon> L_o)^{1/3} = (<\varepsilon> N^{-1})^{1/2}. \qquad (8)$$

where $<\varepsilon>$ is the previously defined average dissipation rate between 1 meter and h_E. Figure 3 shows the shape of turbulent energy spectrum (solid line) and the dissipation spectrum (dotted line) for N=0.001 rad s^{-1} and U_{10}=1, 5, 10 and 20 m sec^{-1} at 61°S. Since N can be an order of magnitude larger than 0.001 Figure 4 is prepared for N=0.01 rad s^{-1} with the same condition. The turbulent eddy sizes vary between the energy containing eddy scale and the Kolmogorov dissipation scale.

Another length scale may be used to describe the turbulence field is the Taylor microscale $l_T \equiv us^{-1}$, where s^2 is a turbulent strain component $2\varepsilon 15^{-1}\nu^{-1}$. The turbulent field may be considered as an equivalent vortex tube with the size of l_T and the velocity scale u. Although the length scale is not a characteristic length of the strain-rate field and does not represent any group of eddy sizes in which dissipative effects are strong (Tennekes and Lumley, 1972, p 68), the scale has a direct implication to the Lagrangian auto-correlation function and thus makes useful to link the universal spectral theory and the diffusion processes.

It is instructive to show an inter-comparison among four length scales. The Ekman depth h_E is shown in Figure 5 (solid line) with the depth averaged dissipation rate, $<\varepsilon>$. The Ozmidov scale L_o (dotted lines), the Taylor microscale l_T (single- and double-chain-dot lines), and the Kolmogorov scale η (dashed line) are also depicted against $<\varepsilon>$. We used three different buoyancy frequency N=0.001, 0.005, 0.01 rad s^{-1} for L_o.

Since the energy containing eddy size can be set by either h_E or L_o, the Taylor microscales based on both scales are shown in the same figure. For the wind speed higher than 5 m s^{-1} these scales hold the inequality $h_E > L_o > l_\tau > \eta$. The Taylor microscale is insensitive to changes in $<\varepsilon>$, in fact l_T base on L_o is independent from $<\varepsilon>$. The range of l_τ is approximately an order of magnitude around 10^{-1} m. Turbulence eddies within the inertia sub-range are unaffected by the size of the energy containing eddy and the viscous dissipation scale. The Ozmidov scale can be considerably different depending on the stratification but the size of largest eddy is limited by the depth of mixed layer h_E.

2.4 Diffusivity

Particle tracking must be done in a Lagrangian fashion, thus the above discussion is not useful unless we relate the universal spectrum to the Lagrangian statistics. A particle displacement can be investigated with the Lagrangian auto-correlation function $\rho_L(\tau)$. The empirical function is in a simple form,

$$\rho_L(\tau) = \exp(-\tau\lambda^{-1}) \qquad (9)$$

where λ is the integral time scale. For this simple form of the auto-correlation function the integral scale is related with the Taylor microscale, namely $\lambda = l_T u^{-1}$ provided the Lagrangian velocity scale is identical to the Eulerian velocity scale. A mean square value of a particle displacement, $<X(t)>^2$, can be expressed in terms of λ.

$$<X(t)>^2 = 2u^2\lambda t. \qquad (10)$$

Note that the above expression is valid as an asymptotic result. The diffusion coefficient K_D can be defined as follows (Taylor, 1921),

$$K_D = (1/2)\, d<X(t)>^2/dt = u^2\lambda = u l_T. \qquad (11)$$

If we employ Eulerian quantities for the above expression we can rewrite K_D as

$$K_D = (15/2)^{1/2} (\varepsilon l^4 \nu^3)^{1/6} \qquad (12)$$

If we take $l = L_o$,

$$K_D = (15/2)^{1/2} (\varepsilon \nu^{-2})^{1/2} = 7.5 \nu s N^{-1}. \qquad (13)$$

Since we used the Ozmidov scale for l the formula is only applicable for the vertical diffusion in the stably stratified environment. The equation (13) is considerably different from the empirically suggested form $K_z = \alpha \varepsilon N^{-2}$ where a is an empirical constant. Osborn (1980) suggests the upper bound for a is 0.2, hence

$$K_z = 0.2 \varepsilon N^{-2}. \qquad (14)$$

Since the diffusion coefficient must have the same dimension with the turbulence velocity scale u times a length scale L, a dimensional argument yields K_z must be a constant times uL. Hence the K_z model can be obtained by setting $L = L_o$. The discrepancy between (13) and (14) is rooted in the original formulation.

Figure 6 shows values of K_D and K_z against ε for three different N (0.001, 0.005 and 0.01 rad s^{-1}). The kinematic viscosity was evaluated at 2°C. The average dissipation rate in the mixed layer is roughly between 10^{-7} and 10^{-6} W Kg^{-1}. Diffusion coefficient from the K_z

model varies three decades between 10^{-4} and 10^{-1} m^2 s^{-1}. On the other hand the K_D model varies 10^{-4} and 10^{-3} m^2 s^{-1}. We think realistic values for the diffusion coefficient may be close to the K_D model.

3 ONE DIMENSIONAL LAGRANGIAN MODEL

3.1 Model

The random walk model is extensively used in simulating particle diffusion and animal aggregation. Skellam (1951) uses the random walk model and the law of diffusion for the study of spatial expansion and distribution of animal population. Our initial step to model the motion of particles follows the conventional random walk. A single particle moves from a position $X(t)$ to an adjacent position $X(t+\Delta t)$ with an instantaneous velocity $V(X,t)$. The cause of movement involves physical, physiological, and social factors. We trace the trajectory of particle every time interval Δt.

$$X(t+\Delta t) = X(t) + \int_{t}^{t+\Delta t} V(X,s)\, ds \qquad (15)$$

where t is a continuous time. The discrete form of the above equation may be written as

$$X(n+\Delta n) = X(n) + Z(n) \qquad (16)$$

where n is an equally spaced discrete time and $Z(n)$ is an appropriate step size over an fixed time interval Δn. If $Z(n)$ is white noise, the process is the pure random walk. It is convenient to separate $Z(n)$ into biologically induced velocity $Z_B(n)$, e.g. swimming or sinking, and physically induced velocity $Z_P(n)$, e.g. mean current or turbulence, namely

$$Z(n) = Z_B(n) + Z_P(n). \qquad (17)$$

We apply a simple random walk diffusion for $Z_P(n)$ if the particle is in the mixed layer, otherwise there is no physical forcing. The step size $Z_P(_n)$ follows a normal distribution with mean zero and standard deviation $(2K_D\Delta n)^{1/2}$. We used K_D=10^{-4} m^2 s^{-1} and Δn=1 800 sec (30 minutes). These diffusion coefficients are approximately for cases U_{10}=10 m s^{-1} with N=0.01 (see Figure 6) The biological component, $Z_B(n)$, is a constant-speed. The organisms do not interact with each other so that each particle can be traced independently. The depth of mixed layer is set by the Ekman layer model and the turbulent diffusion only happens in the mixed layer with uniform intensity.

3.2 Simulations

At the beginning of the simulation 1 000 particles are located at the surface. Presumably phytoplankton continuously produce new generations. Thus, 1000 particles are added at every 24 hours over 10 day simulation time. At the end of the simulation 11 000 particles were traced. Table 1 summarizes simulation cases.

Figure 7 shows a series of particle distribution profiles at every 12 hours. Particles diffuse like a continuous medium within the mixed layer. No significant change in the density of particle was observed below the mixed layer, 38m, for this case. A slight increase in the descending speed of particle cause drastic difference in the distribution (Figure 8). Because particles sink faster than diffusive effect of turbulence, particles are grouped in a single cluster for each generation. For descending particles under weak wind

condition, U_{10}=5 m s^{-1}, a deposit of particles can be found at the base of mixed layer, however, once a particle leaves the turbulent region it never get back to the mixed layer (Figure 9). These results indicate that fast sinking particles distribute rather uniformly inside and below the mixed layer. On the other hand, if the turbulent intensity is not strong enough in the mixed layer for fast sinking particles a non-uniform distribution of particles is created.

Finally, some species of phytoplankton can swim upward and the slight motile may cause a significant difference in the life stage. Due to the active swimming a particle can be entrained back to the mixed layer even if it has been left from the mixed layer. An example of particle trajectory is shown in Figure 10. Although a deposit of particles at the base of mixed layer is growing with time, members of the cluster can be changed over the time. Physiologically this mechanism may act to reduce photo-inhibition. Woods and Onken (1982) showed a particle re-entry mechanism into the mixed layer by introducing diurnal convective mixing. As we have discussed in section 2.2 the diurnal changes in the depth mixed layer is seeming unlikely in the Antarctic ocean.

4. SUMMARY

Our simulation is still in an early stage. No suggestions can be made relating to the distribution of krill. However, we demonstrated the distribution of phytoplankton can be significantly changed depending on the depth mixed layer, the level of turbulence and the sinking/swimming speed of particle. The upper layer in the Antarctic ocean is not as well mixed as we originally thought. Presumably the weak mixing condition allows the phytoplankton to grow sufficiently with almost unlimited nutrition level. Interrelation between physical processes and the primary productivity in the upper ocean must have unique characteristics in the Antarctic ocean.

REFERENCES

BOYD, C.M., M. HEYRAUD and C.N. BOYD. 1984. Feeding of the Antarctic Krill *Euphausia Superba*. Journal of Crustacean Biology 4 (Spec. 1): 123-141.

GARGETT, A.E., T.R. OSBORN and P.W. NASMYTH. 1984. Local isotropy and the decay of turbulence in a stratified fluid. Journal of Fluid Mechanics 144: 231-280.

GORDON, A.L. 1988. Physical oceanographic setting the *Seidlecki* January 1987, South Shetland Island data set, in draft.

GREGG, M.C. 1987. Structures and fluxes in a deep convecting mixed layer. Dynamics of the oceanic surface mixed layer, Proceeding of Hawaiian Winter Workshop, University of Hawaii at Manoa, January 14-16, 1987: 1-24.

HAN, Y.-J., and S.-W. LEE. 1981. A new analysis of monthly mean wind stress over the global ocean, Rep. 26, Climate Research Institute, Oregon State Univ., Corvallis: 148 pp.

LUECK, R.G. 1989. Near surface turbulence during the passage of a storm, in draft.

MORRIS, D.J., I. EVERSON, C. RICKETTS and P. WARD. 1984. Feeding of krill around South Georgia. II. Relations between feeding activity, environment and vertical distribution Marine Ecology -Progress Series 20: 203-206.

MOUM, J.N., D.R. CALDWELL. 1985. Local influences on shear-flow turbulence in the

equatorial ocean. Science 230: 315-316.

OSBORN, T.R. 1980. Estimates of the local rate of vertical diffusion from dissipation measurements. Journal of Physical Oceanography 10: 83-89.

ROSS, R.M.. and L.B. QUETIN. 1986. How Productive are Antarctic Krill? BioScinec 36: 264-269.

PLATT, T. and C.L. GALLEGOS. 1980. Modeling primary production. Primary Production in the Sea. FALKOWSKI, P.G. (ed.). Plenum Press, p 339-362.

SKELLAM, J.G. 1951. Random dispersal in theoretical population. Biometrika 38: 196-218.

TENNEKES, H and J.L. LUMLEY. 1972. A First Course in turbulence. MIT press, Cambridge, Massachusetts, 300 pp.

WEBER, L.H. and S.Z. EL-SAYED. 1985. Spatial variability of phytoplankton and the distribution and abundance of krill in the Indian sector of the South Ocean. In SIEGFRIED, W.R., P.R. CONDY, and R.M. LAWS (Eds). Antarctic Nutrient Cycles and Food Webs p 284-293.

WOODS, J.D. and R. ONKEN. 1982. Diurnal variation and primary production in the ocean - preliminary results of a Lagrangian ensemble model. Journal of Plankton Research 4: 735-756.

WROBLEWSKI, J.S. 1982. Interaction of currents and vertical migration in maintaining callanus marshalae in the Oregon upwelling zone - a simulation. Deep-sea Research 29: 665-686.

Table 1: Physical and biological condition for simulations. Swimming (or sinking) speed, W_B, was kept throughout the simulation for each case. The diffusion coefficient K_D was fixed for all simulations. The value is close to a case when wind speed U_{10} is roughly 10 m s^{-1}. Depth of mixing layer was determined from Ekman layer mode.

Case	*A*	*B*	*C*	*D*
W_B (m s^{-1})	10^{-4}	$3.x10^{-4}$	10^{-5}	-10^{-5}
K_D (m^2s^{-1})	10^{-4}	10^{-4}	10^{-4}	10^{-4}
U_{10}(m s^{-1})	10	10	5	5
h_E (m)	38	38	19	19

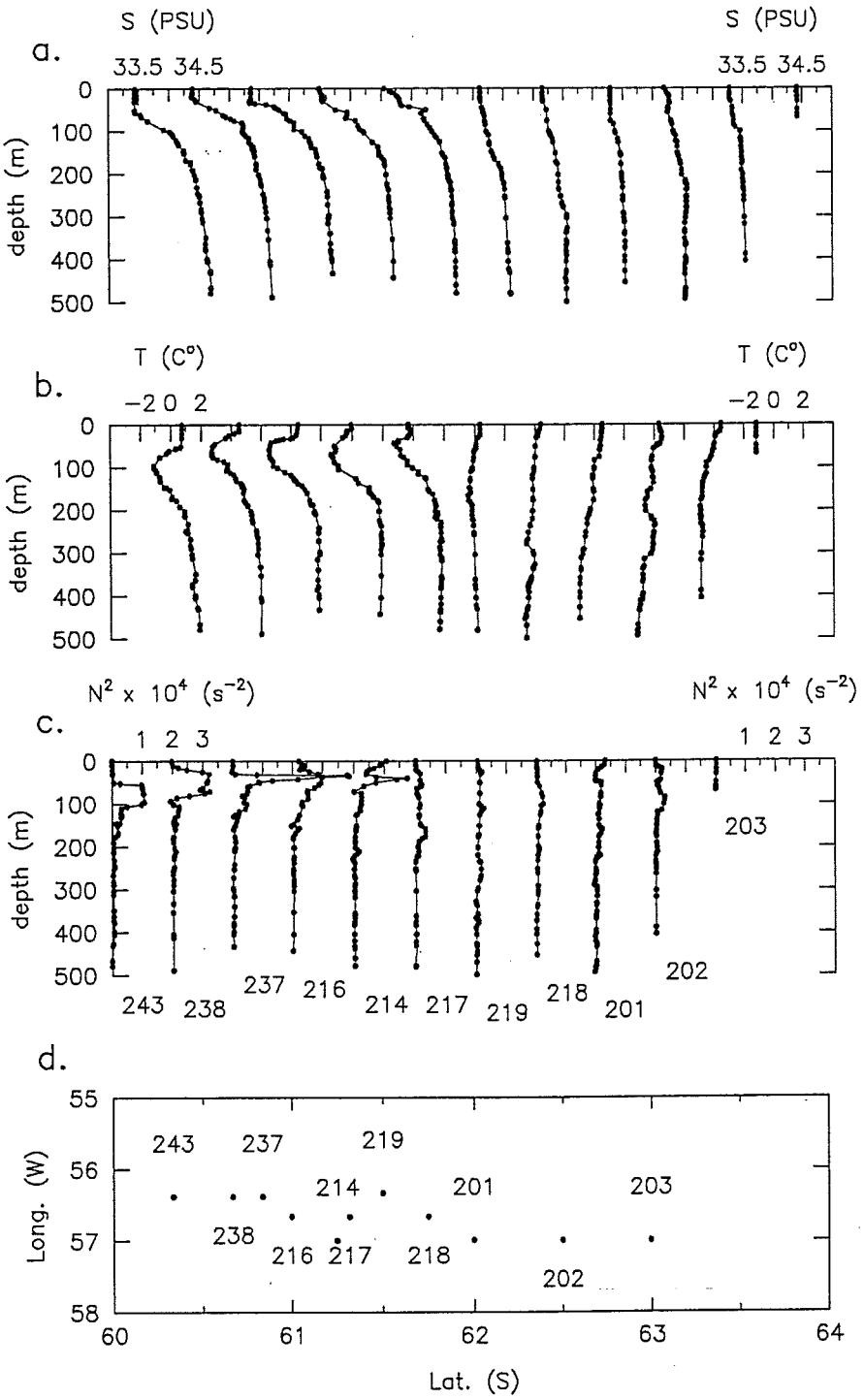

Figure 1: STD profiles along 57°W taken by R/V *Professor Seidlecki* in January 1987. a) Salinity (*S*) profiles. b) Temperature (*T*) profiles. c) Buoyancy frequency (*N*) profiles. d) Location of STD stations. STD station number is shown beneath buoyancy frequency profile.

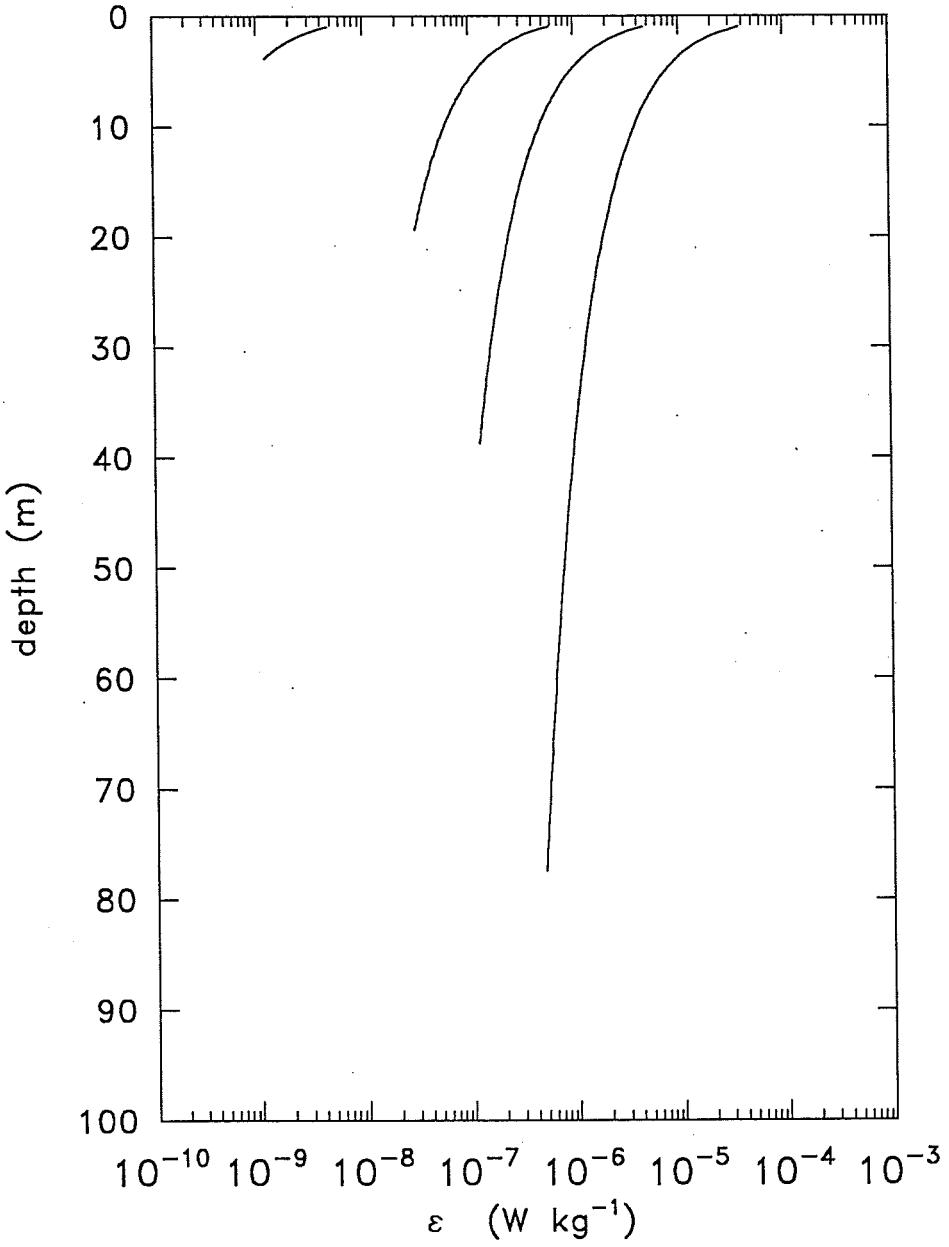

Figure 2: Dissipation profiles between 1 m and the base of the Ekman layer at 61°S. Four wind conditions are used; U_{10} = 1, 5, 10 and 20 m/sec (from the left to the right of profiles).

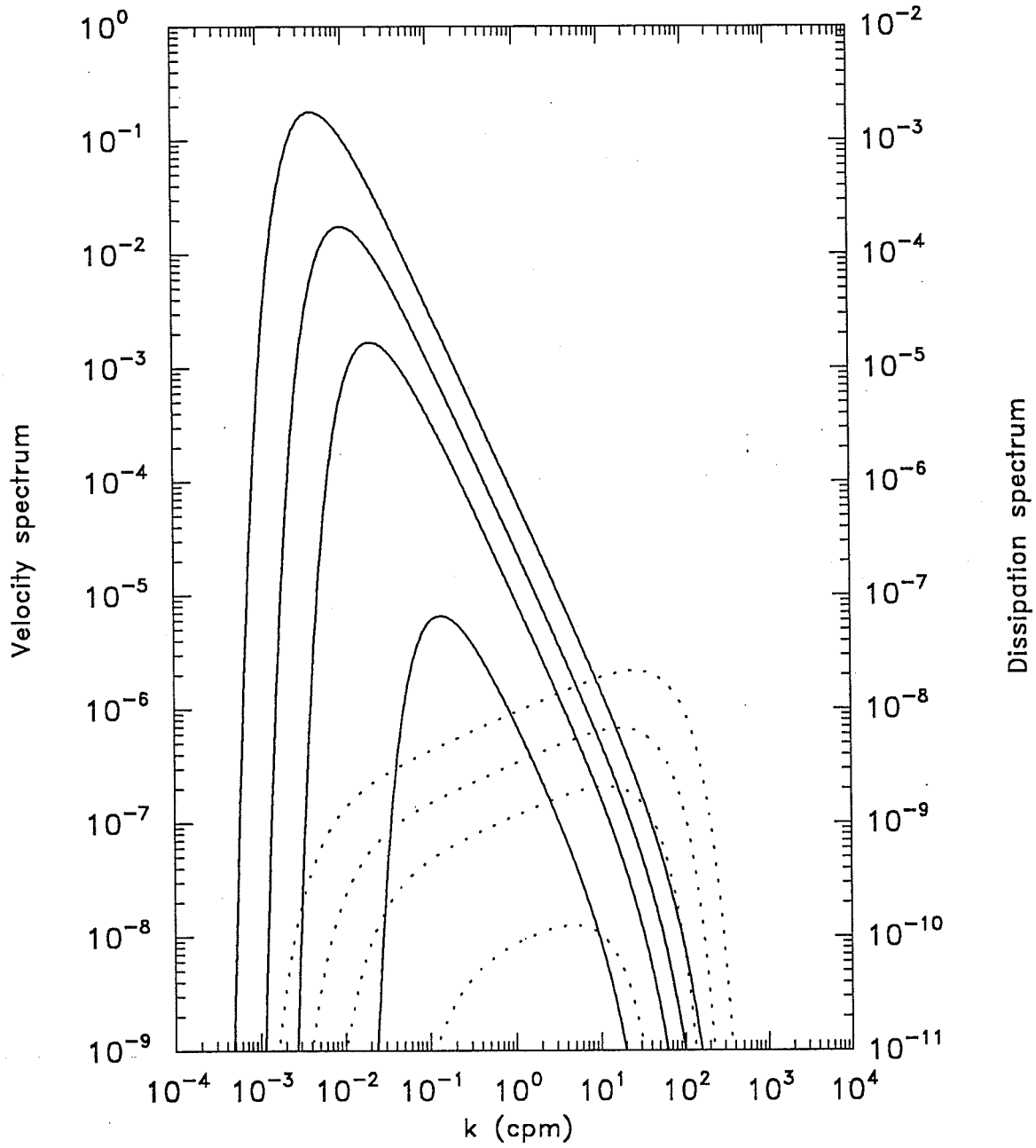

Figure 3: Turbulence velocity spectra (solid lines) and dissipation spectra (dotted lines). The dissipation rates are set by the average dissipation rate from Ekman layer model. Four different wind speeds are used U_{10}=20, 10, 5, and 1 m s^{-1} (from the top to the bottom). The energy contained eddy size is set by the Ozmidov scale $L_o=(\varepsilon N^{-3})^{1/2}$ where N=0.001 rad s^{-1} is used.

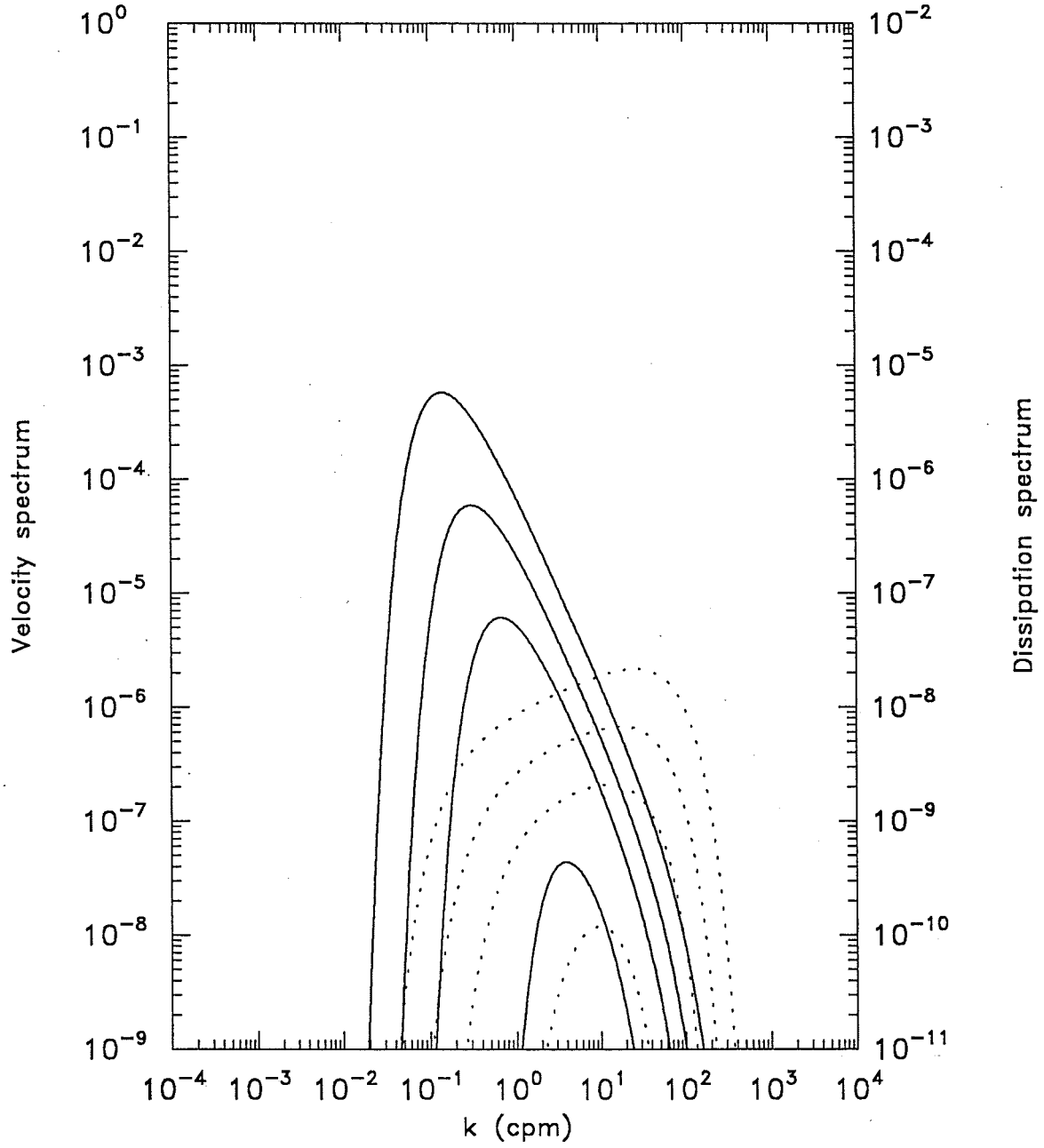

Figure 4: Same as Figure 3 with N=0.01 rad s^{-1}.

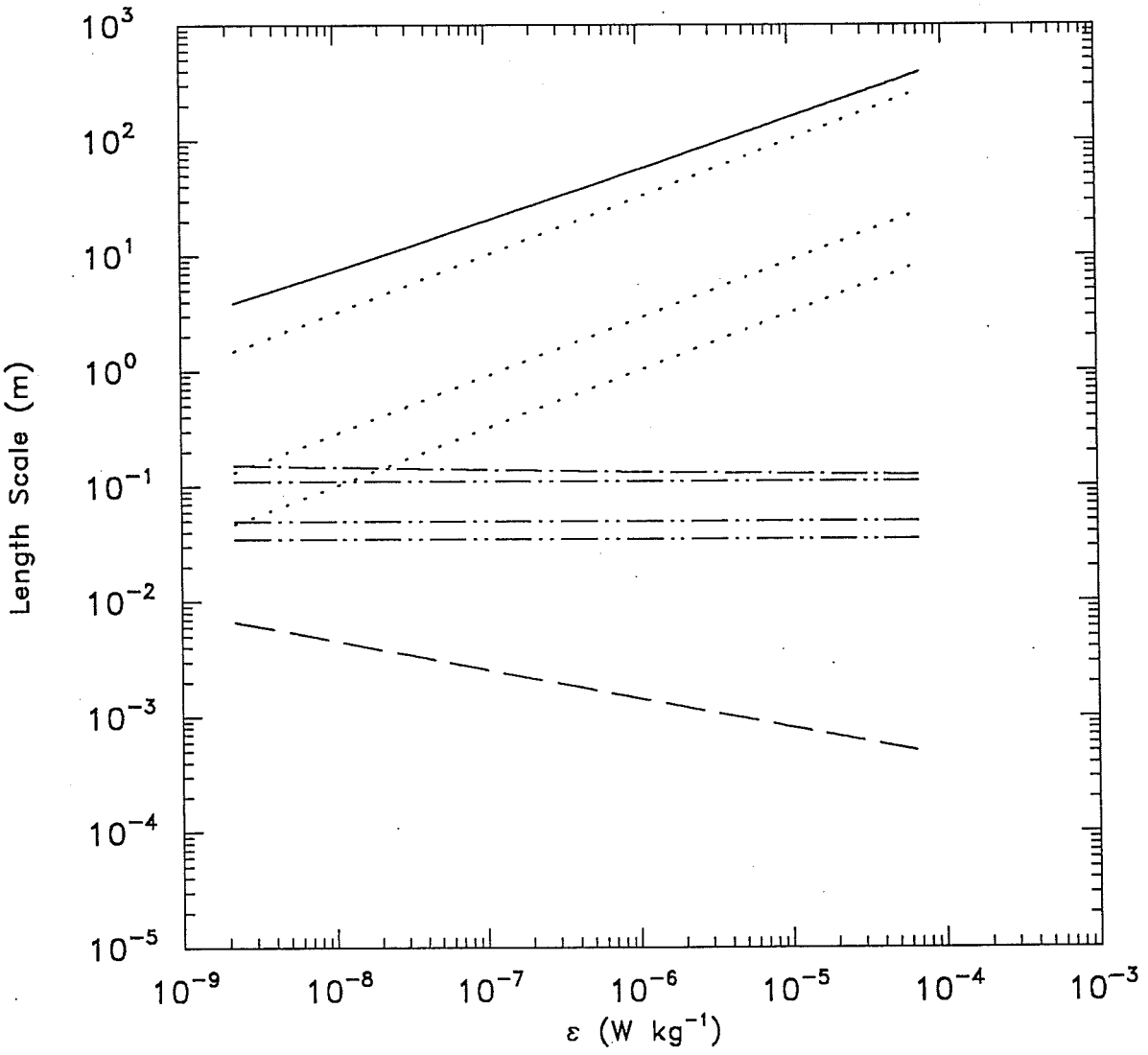

Figure 5: Length scales against dissipation rate. The Ekman layer depth is shown by a solid line and the dissipation rate associated with the length scale is the depth average value. The Ozmidov scale is calculated with three different N=0.001, 0.05 and 0.01 rad s^{-1} and three cases are shown by dotted lines (from the top to the bottom). The Taylor microscale depends on the energy containing eddy size. Two cases are shown the figure. The microscale based on the Ekman depth is shown by single chain dot and the Taylor microscale calculated from the Ozmidov scale appears as three lines of chains with double dots for N=0.001, 0.05 and 0.01 from the top line to the bottom line respectively. The Kolmogorov scale is depicted with a dashed line.

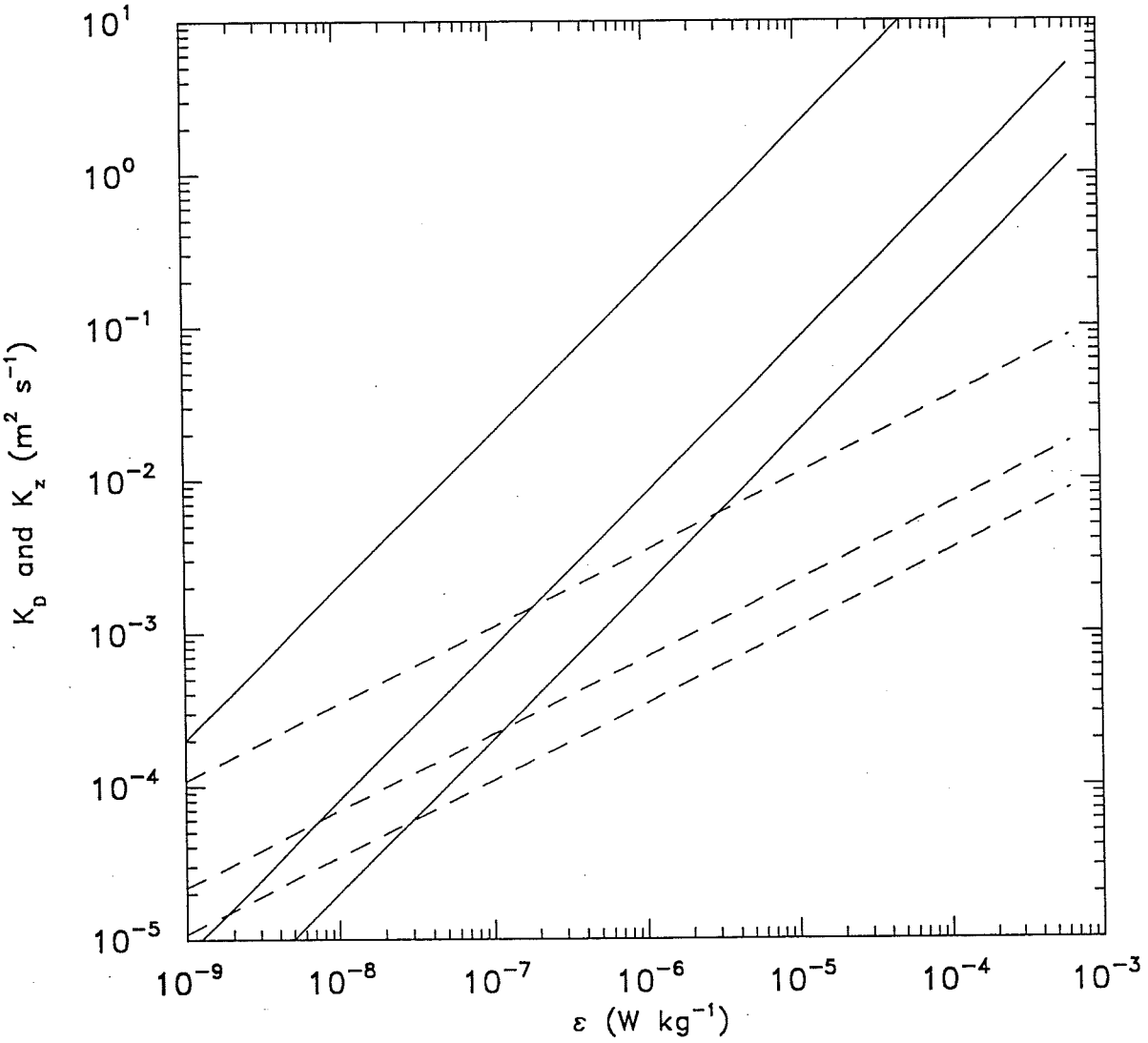

Figure 6: Two diffusion coefficient estimates K_D and K_z against dissipation rates. Solid lines show K_z and dotted lines are K_D. Three different N are used. The top of each line is N=0.001. The middle is N=0.05. The bottom is N=0.01.

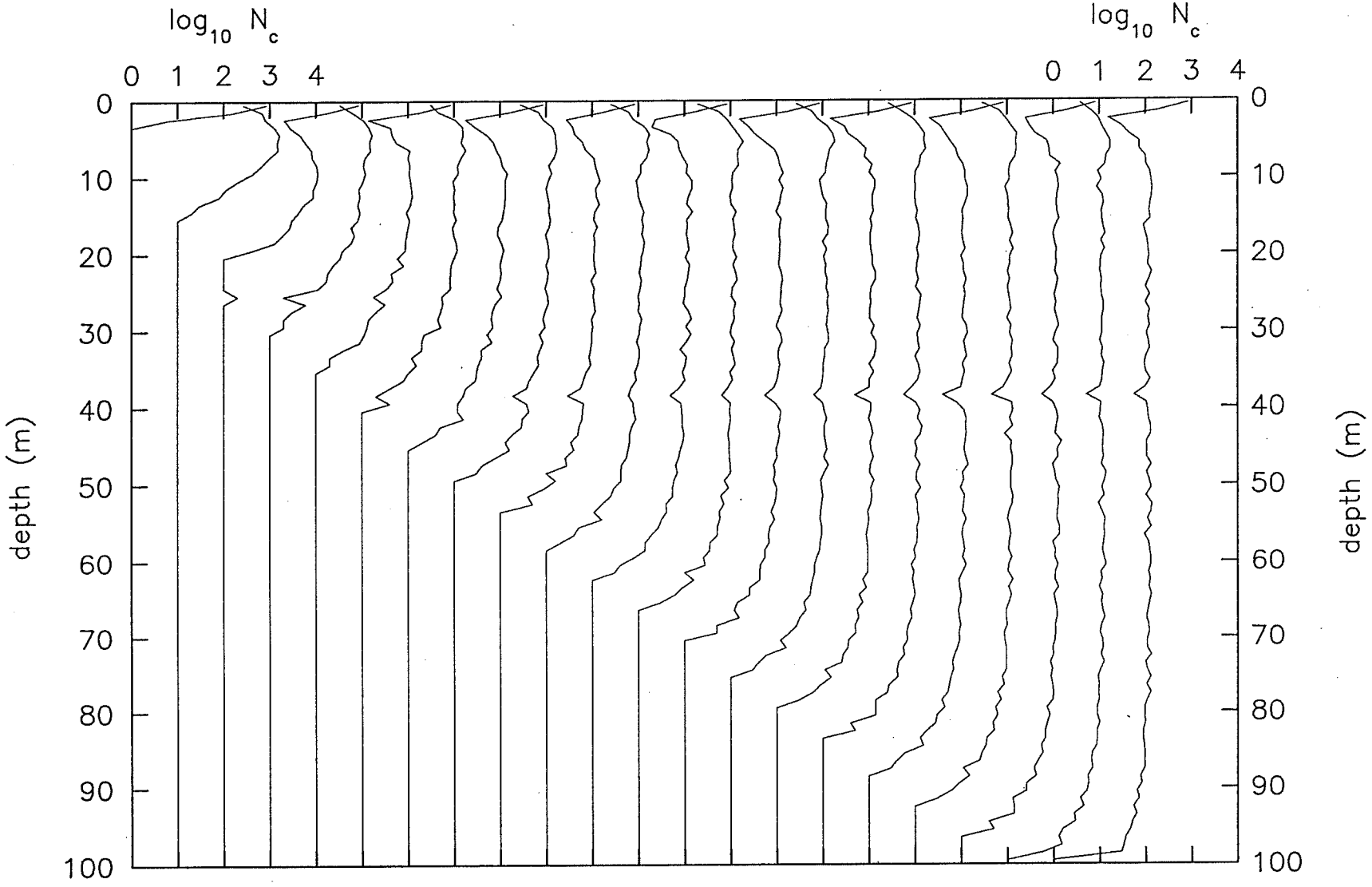

Figure 7: Particle distribution profiles at every 12 hours. Number of particles, N_c, in one-meter bin is shown in logarithmic scale base 10. Each profile offsets by one decade. Simulation Case *A*.

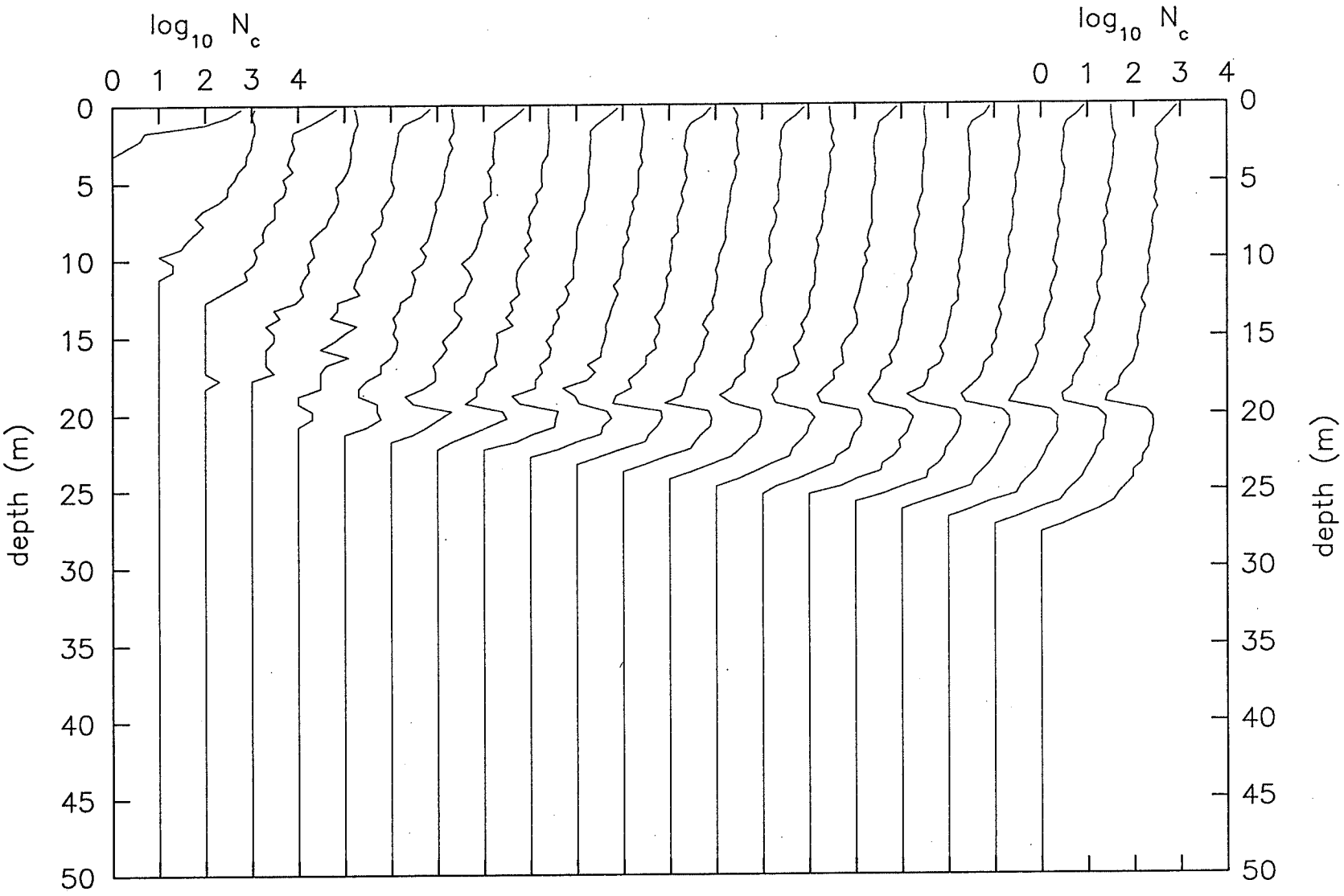

Figure 8: Same as Figure 7 for simulation Case *B*.

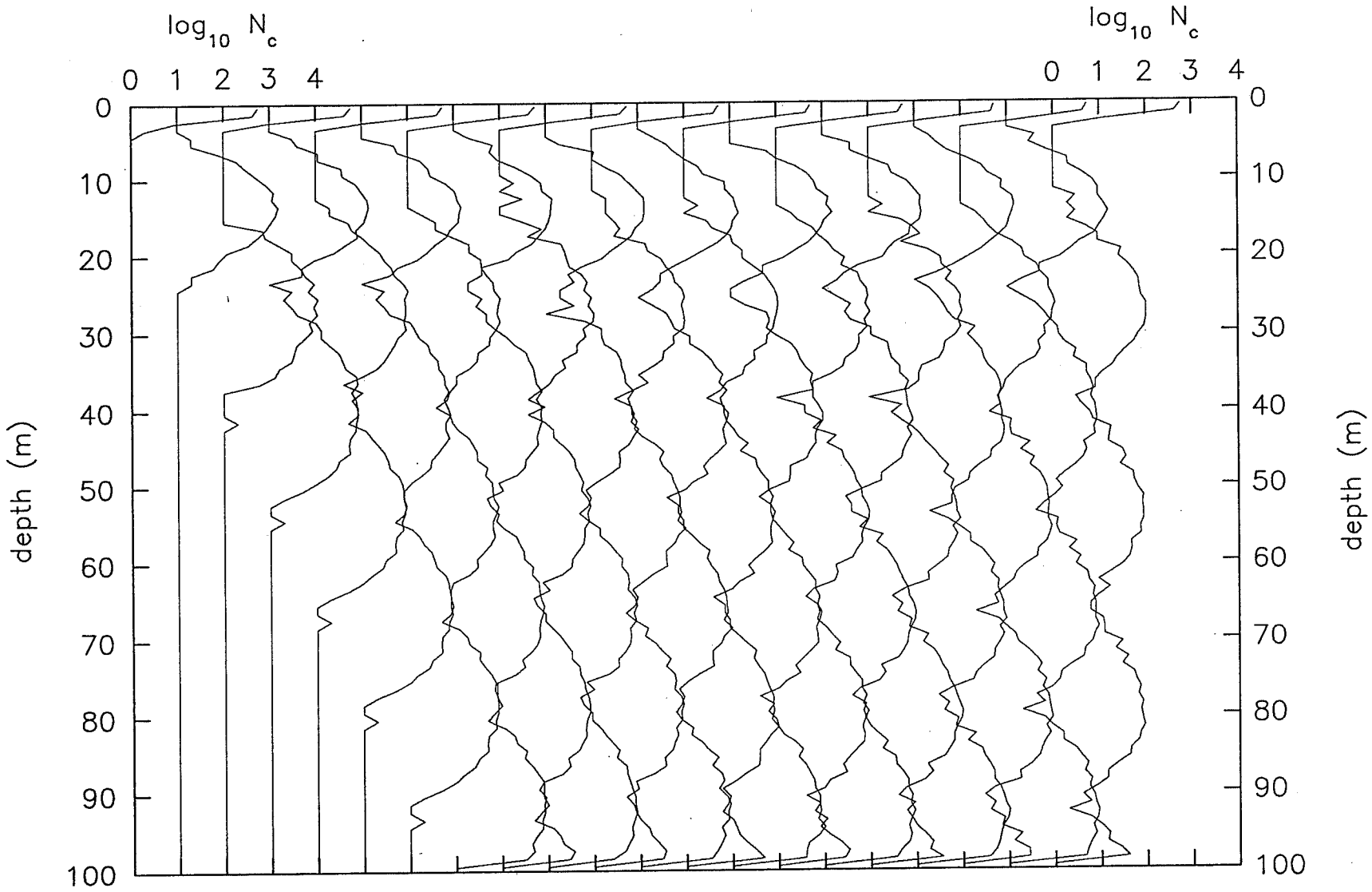

Figure 9: Same as Figure 7 for simulation Case *C*.

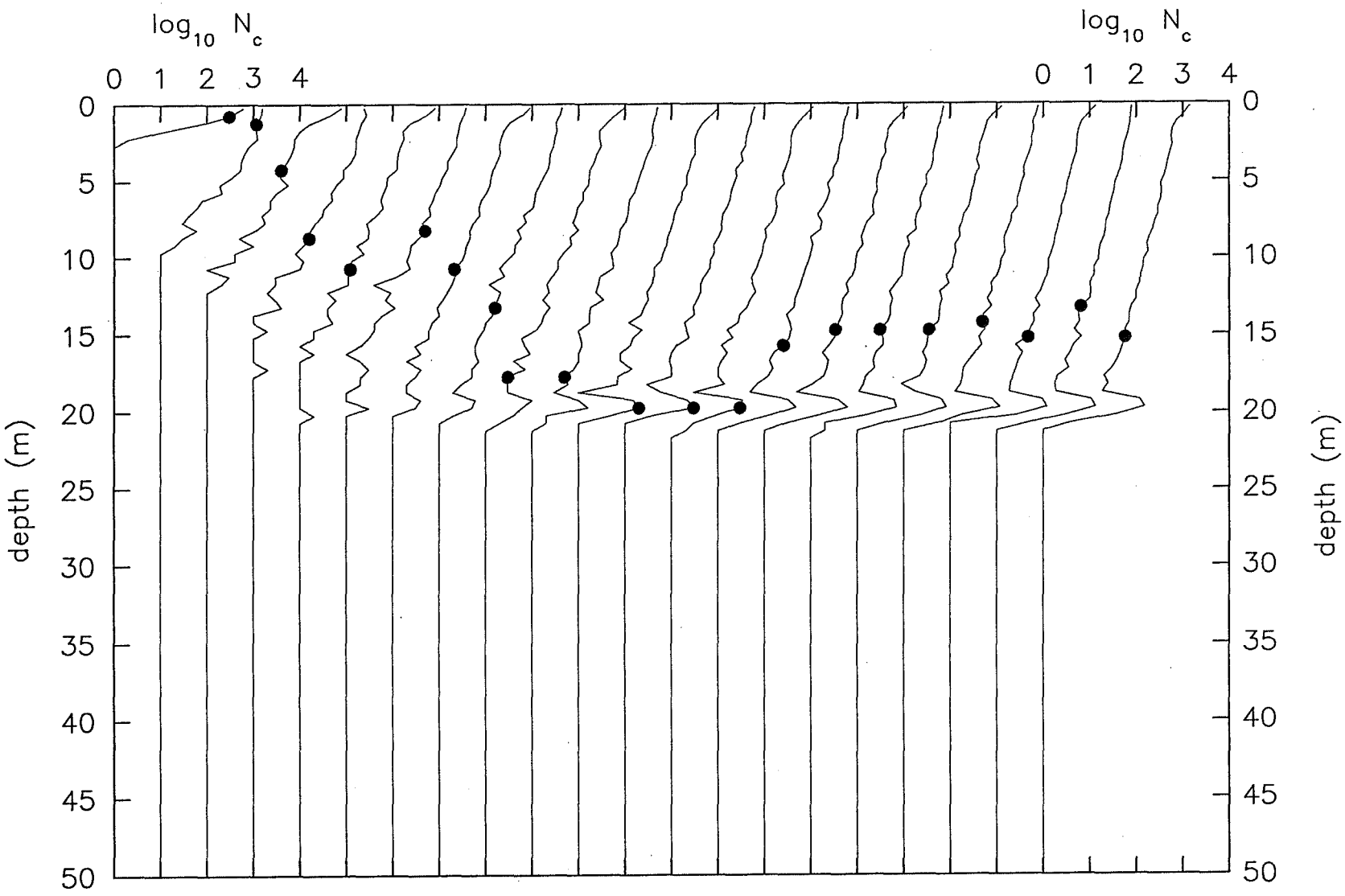

Figure 10: Same as Figure 7 for simulation Case *D*. Solid circles show trajectory of a particle over the whole simulation. The particle leaves the mixed layer roughly after 5 days and is trapped in the base of the mixed layer for a day and half. The particle, then, successfully re-enters in the mixed layer and stays in the mixed layer for the rest of the simulation period.

Légende du tableau

Table 1 — Conditions physique et biologique pour les simulations. La vitesse de nage (ou d'enfoncement) W_B, était constante pour toute la simulation dans chaque cas. Le coefficient de diffusion K_D était fixe dans toutes les simulations. La valeur est proche de celle d'un cas où la vitesse du vent U_{10} serait d'environ 10 m/s. La profondeur de la couche de mélange a été déterminée d'après le modèle de couche d'Ekman.

Légendes des figures

Figure 1 — Courbes de salinité / température / profondeur le long de 57°O relevées par le navire de recherche *Professor Siedlecki* au mois de janvier 1987. a) Courbes de salinité (S). b) Courbes de température (T). c) Courbes de fréquence de flottabilité (N). d) Emplacement des stations de salinité / température / profondeur Le numéro de la station de salinité / température / profondeur est indiqué sous la courbe de fréquence de flottabilité.

Figure 2. — Courbes de dispersion entre 1 m et la base de la couche Ekman à 61°S. Quatre conditions de vents différents ont été utilisées; U_{10} = 1, 5, 10 et 20 m/sec (de la gauche à la droite des courbes).

Figure 3 — Spectres de la vitesse de la turbulence (lignes continues) et spectres de dissipation (lignes en pointillé). Les taux de dissipation sont fixés au taux moyen de dissipation du modèle des couches d'Ekman. Quatre vitesses de vent différentes ont été utilisées; U_{10} =1, 5, 10 et 20 m/sec^1. L'énergie a été calculée en tenant compte de la taille du remous, et est fixé par l'échelle Ozmidov $L_o = (eN/^3)^{1/2}$ où N = 0.001 rayon/sec est utilisé.

Figure 4 — Identique à la figure 3 avec N = 0.01 rayon sec^{-1}.

Figure 5 — Echelles de longueur en fonction du taux de dissipation. La profondeur de la couche Ekman est indiqué par une ligne continue et le taux de dissipation associé avec l'échelle de longueur est la valeur moyenne de profondeur. L'échelle Ozmidov est calculée avec trois différents N = 0.001, 0.05 et 0.01 rayon/sec et trois cas sont indiqués par des lignes pointillées. La micro-échelle Taylor dépend de l'énergie calculée en tenant compte de la taille du remous. Deux cas sont illustrés sur la figure. La base de la micro-échelle sur la profondeur Ekman est indiqué par un pointillé simple et les échelles avec les échelles Ozmidov apparaissent en pointillé double. L'échelle Kolmogorov est representée par une ligne tiretée.

Figure 6 — Deux estimations du coefficient de diffusion K_D et K_z en fonction de taux de dissipation. Les lignes continues indiquent K_z et les lignes pointillées, K_D. Trois N différents sont utilisés. Le haut de chaque ligne est N = 0.001. Le centre est N = 0.05. Le bas est N = 0.01.

Figure 7 — Courbes de distribution des particules toutes les 12 heures. Le nombre de particules, N_c dans un réceptacle d'un mètre est indiqué sur une échelle logarithmique de base 10. Chaque courbe représente la situation de 10 jours en 10 jours. Cas de simulation *A*.

Figure 8. — Identique à la figure 7 pour le cas de simulation *B*.

Figure 9. Identique à la figure 7 pour le cas de simulation *C*.

Figure 10. Identique à la figure 7 pour le cas de simulation *D*. Les cercles pleins montrent la trajectoire d'une particule sur toute la simulation. La particule quitte la couche mixte après environ 5 jours et est bloquée à la base de la couche mixte pour un jour et demi. Ensuite, la particule réussit à rentrer dans la couche mixte et y reste pendant le reste de la période de simulation.

Заголовки к таблицам

Таблица 1 Физические и биологические условия моделирования. Скорость плавания (или погружения), W_B была постоянной для случаев моделирования. Коэффицент рассеивания K_D был постоянным для всех прогонов модели. Его значение близко к случаю, когда скорость ветра U_{10} равнялась приблизительно 10 м/сек. Глубина смешивающего слоя была определена по модели слоя Экмана.

Подписи к рисункам

Рисунок 1 Профили STD вдоль 57°з.д., взятые НИС "Профессор Седлецкий" в январе 1987 г. a) Профили солености (*S*). b) Профили температуры (*T*). c) Профили частоты встречаемости слоя с нейтральной плавучестью (*N*). d) Местонахождение станций STD. Номера станций STD показаны под профилем частоты встречаемости слоя с нейтральной плавучестью.

Рисунок 2 Профили рассеивания между 1 м и основанием слоя Экмана на 61° ю.ш.Используются четыре условия ветра; U_{10} = 1, 5, 10 и 20 м/сек (слева направо по направлению профилей).

Рисунок 3 Спектр скоростей турбулентности (непрерывные линии) и спектры рассеивания (точечные линии).Коэффициенты рассеивания усреднены по модели слоя Экмана. Используется четыре скорости ветра; U_{10} = 1, 5, 10 и 20 м/сек. Отношение между энергией и размером водоворота составлено по шкале Озмидова $L_O = (\varepsilon/N^3)^{1/2}$, где N=0,001 рад/сек.

Рисунок 4 То же, что изображено на рисунке 3, но в данном случае N=0,01 рад/сек.

Риунок 5 Шкалы длины по отношению к коэффициенту рассеивания. Непрерывная линия указывает глубину слоя Экмана, и коэффициент рассеивания, связанный со шкалой длины, является средним значением глубины. Шкала Озмидова рассчитана по трем разным значениям: N = 0,001, 0,05, и 0,01 рад/сек. Три случая показаны точечными линиями. Микромасштаб Тейлора зависит от размера содержащейся в водовороте энергии. На рисунке представлены два примера. Микромасштаб, основанный на глубине слоя Экмана, отмечен штрих-пунктирной линией и масштабы, основанные на шкале Озмидова, изображаются двойной штрих-пунктирной линией. Шкала Колмогорова изображается пунктирной линией.

Рисунок 6 Две оценки коэффициента распространения K_D и K_Z по отношению к коэффициенту рассеивания. Заштрихованные точки указывают K_Z и точечные линии - K_D Используются три разных N. Верхней точкой каждой линии является N=0,001. Средней точкой - N = 0,05. Нижней точкой - N = 0,01.

Рисунок 7 Профили распределения частиц через каждые 12 часов. Количество частиц N_c в одометровой ячее показано на логарифмической шкале (lg). Расстояние между профилями равно 10 дням. Случай моделирования Фб

Рисунок 8 То же, что на рисунке 7 для случая моделирования *B*.

Рисунок 9 То же, что на рисунке 7 для случая моделирования *C*.

Рисунок 10 То же, что на рисунке 7 для случая моделирования *D*. Заштрихованные точки показывают траекторию частицы в течение всего моделирования Частица покидает смешивающий слой приблизительно через 5 дней и задерживается в основании смешивающего слоя на полтора дня. Затем частица успешно снова входит в смешивающий слой и остается там до окончания периода моделирования.

Encabezamiento de la Tabla

Tabla 1 Condiciones físicas y biológicas para simulaciones. La velocidad de natación (o hundimiento), W_B, se mantuvo durante la simulación de cada caso. Se fijó el coeficiente de difusión K_D para todas las simulaciones. El valor está próximo a un caso cuando la velocidad del viento U_{10} es aproximadamente 10 m s^{-1}. La profundidad de la capa mixta fue determinada a partir de la moda de la capa Ekman.

Leyendas de las Figuras

Figura 1a Perfiles STD (salinidad, temperatura, profundidad) a lo largo de los 57°O tomados por el B/I *Professor Siedlecki* en enero de 1987. a) Salinidad (S) perfiles. b) Temperatura (T) perfiles. c) Frecuencia de flotabilidad (N) perfiles. d) Localización de las estaciones STD. El número de estación STD se muestra debajo del perfil de frecuencia de flotabilidad.

Figura 2 Perfiles de disipación entre 1 m y la base de la capa Ekman a los 61°S. Se usan cuatro condiciones de viento; U_{10} = 1,5,10, y 20 m sec^{-1} (de izquierda a derecha de los perfiles).

Figura 3 Espectro de velocidad de turbulencia (líneas sólidas) y espectro de disipación (líneas de puntos). Los índices de disipación se establecen por el índice de disipación promedio del modelo de la capa Ekman. Se utilizan cuatro velocidades de viento diferentes U_{10} = 1,5,10 y 20 m sec^{-1}. La energía contenida en un remolino de un tamaño dado se establece por la escala Ozmidov $L_o = (N^{-3})^{1/2}$ donde N = 0.001 rad sec^{-1} es utilizado.

Figura 4 Igual que en la Figura 3 con N = 0.01 rad sec^{-1}.

Figura 5 Escala de longitud como función del índice de disipación. La profundidad de la capa Ekman está indicada con una línea sólida y el índice de disipación asociado con la escala de longitud es el valor promedio de profundidad. La escala Ozmidov se calcula con tres N = 0.001, 0.05 y 0.01 rad sec^{-1} diferentes y tres casos están indicados mediante líneas de puntos. La micro escala Taylor depende de la energía que contiene remolinos de un tamaño dado. Se muestran dos casos en la Figura. La base de la micro escala en la profundidad Ekman está indicada por una cadena de puntos sencilla y las escalas Ozmidov aparecen con una cadena de puntos doble. La escala Kolmogorov está representada con una línea quebrada.

Figura 6 Dos estimaciones del coeficiente de difusión K_D y K_Z en relación a los índices de disipación. Las líneas sólidas representan K_Z y las líneas de puntos K_D. Se utilizan tres N diferentes. La parte superior de cada linea es N = 0.001. La parte central es N = 0.05. La parte inferior es N= 0.01.

Figura 7 Perfiles de la distribución de partículars cada 12 horas. Caso de simulación *A*.

Figura 8 Perfiles de la distribución de partículas cada 12 horas. Caso de simulación *B*.

Figura 9 Perfiles de la distribución de partículas cada 12 horas. Caso de simulación *C*.

Figura 10 Perfiles de la distribución de partículas cada 12 horas. Caso de simulación *D*.